

ANALYSIS OF LAMINAR BOUNDARY-LAYER FLOW OVER A MOVING WEDGE USING A UNIFORM HAAR WAVELET METHOD

Harinakshi Karkera^a, Nagaraj N. Katagi^{a,†}, Ramesh B. Kudenatti^b

^aDepartment of Mathematics, Manipal Institute of Technology, Manipal Academy of Higher Education, Manipal, 576 104, India

^bDepartment of Mathematics, Bengaluru City University, Bengaluru, 560 001, India

ABSTRACT

In this paper, we study the characteristics of laminar boundary-layer flow of a viscous incompressible fluid over a moving wedge. The transformed boundary-layer equation given by the Falkner-Skan equation is solved by an efficient easy-to-use approximate method based on uniform Haar wavelets in conjunction with quasilinearization and collocation approach. The residual and error estimates are computed to confirm the validity of the obtained results. A meaningful comparison between the present solutions with existing numerical results in the literature is carried out to highlight the benefits and efficiency of proposed method. Furthermore, the influence of variable pressure gradient and the wedge velocity parameter are discussed and illustrated through graphs. The Haar wavelet approach discovers a rich structure of multiple solutions for various range of physical parameters.

Keywords: Boundary-layer; Moving wedge; Nonlinear boundary value problem; Multiple solutions; Haar wavelets.

1. INTRODUCTION

The two-dimensional laminar boundary-layer flows of a viscous and incompressible fluid over a wedge surface are fundamental for the understanding of aerodynamical properties of the fluid flow, and have applications in engineering and technology such as aerodynamic extrusion of plastic sheets, cooling of a metallic plate in a cooling bath, fibre processing, magnetic tape production, etc. When the mainstream fluid with a large Reynolds number (will be defined later) flows over a wedge surface, the effects of viscosity are confined to a thin layer near the wedge surface. In many situations, the wedge is considered to move along or opposite (Riley and Weidman (1989), Sachdev *et al.* (2008), etc.) to the mainstream flow or in a still fluid (the mainstream is held constant). The velocity field develops downstream (former case) and upstream (latter case) in the boundary-layer. In the above applications, for example, the plastic sheets or polymer sheets act as a moving wedge with a non-uniform velocity in a still fluid (Wang (1984), Ariel (1994, 2007), Takhar *et al.* (2001)). Such a flow phenomenon is more practical in understanding the properties of the flow.

It is shown in Sachdev *et al.* (2008) that the mainstream flow is approximated in the form x^n (defined later) which is connected to the pressure gradient since the pressure gradient throughout the flow field is assumed uniform. Then the boundary-layer flow problem given by the Falkner-Skan equation admit a class of self-similar solutions which involve the accelerated and decelerated flows along with the Blasius flow. It is also further assumed that the wedge movement is approximated in the form of power-law manner. Thus, numerical treatment of the Falkner-

Skan problem in which the wedge is considered to move opposite to the mainstream flow is given in Riley and Weidman (1989). They found numerically that the multiple solutions are possible for some extreme values of power-law parameter. Liao (1999) obtained an accurate solution in terms of uniformly valid convergent series solution namely homotopy analysis method (wedge is at rest). Sachdev *et al.* (2008) made an analysis to the Falkner-Skan problem along with wedge moving and gave an exact solution to all values of power-law parameter. The various aspects of the Falkner-Skan equation have been solved using Chebyshev pseudo spectral method (Srinivasacharya and Jagadeeshwar (2017)), the Differential transform method (Rashidi and Erfani (2011)), Keller-box method (Ishak *et al.* (2007)), Homotopy analysis method (Abdelmeguid (2017)), Finite difference method (Govindaraj *et al.* (2020)) etc. In fact, the analysis of boundary-layer flow of Newtonian/non-Newtonian fluid models associated with heat transfer, porous stretching medium, thermal radiation etc., has been addressed extensively in the recent literature due to its important impacts on the behaviours of the fluid flow (Bhattacharyya (2012); Kumaresan and Kumar (2017); Ganapathirao *et al.* (2019))

Wavelet analysis is a new branch of applied mathematics which is widely applied in signal analysis, image processing, numerical analysis, etc. These methods have been proved to be robust and elegant tool for most of the mathematical problems. Wavelets allow us to represent a function in the form of a set of bases function which are localised. In this case, Daubechies wavelets (Daubechies (1992)) are used quite often in the solution of non-linear problems. The Daubechies wavelets are orthogo-

[†]Corresponding author. Email: nn.katagi@manipal.edu

nal and sufficiently smooth, but cannot be expressed in terms of explicit function that makes the differentiation and integration quite complicated. Thus, Alfred Haar introduced a concept of Haar wavelet which has an analytic expression and is made up of pairs of piecewise functions, can be integrated any number of times (Daubechies (1992)). In the recent past, the Haar wavelets are proved to be playing an important role in the solution of mathematical problems, particularly the nonlinear ones, (Lepik (2006); Mansoori and Nazemi (2016); Erfanian et al. (2017); Mittal and Pandit (2017); Majak et al. (2018); Ratas et al. (2021a,b); Sorrenti et al. (2021); Mehrparvar et al. (2022)).

The Haar wavelet method in conjunction with quasilinearization procedure has acquired a lot of credence in tackling the non-linear boundary value problems, as the nonlinear nature of these problems impedes its exact solution in most cases. Kaur et al. (2011) proposed a modified Haar wavelet method by introducing the quasilinearization approach to overcome the difficulties in solving the nonlinear boundary value problems. Followed by this, Saeed and Rehman (2013) and Kaur et al. (2014) have successfully used the Haar wavelet with quasilinearization technique mainly for the solution of nonlinear fractional differential and oscillator equations respectively. Later, Jiwari (2015) applied this approach for the approximate solution of time dependent non-linear Burgers' equation. Most of them have, however, considered only the problem of finite domain. We endeavour to extend this method to examine the results for higher order non-linear boundary value problems with semi-infinite or infinite domains and thus making the method more useful in real-world applications.

The main idea of the Haar wavelets is to convert the differential equation into a set of algebraic equations which are solved by inversion technique. In the process of conversion, all boundary conditions (even derivative conditions) are enforced directly into the system (Lepik (2005, 2008)). We note here that the two-dimensional boundary-layer flow over a moving wedge is defined on an infinite domain. But Haar wavelet is defined on $[0, 1]$. Therefore, to overcome this difficulty of infinite domain, we simplify the problem by coordinate transformation and changing of variables and new variables are now defined on $[0, 1]$. For details, see Section 4. This gives a good deal of mathematical simplification in which the variable domain $[0, \infty)$ becomes fixed interval $[0, 1]$. We will continue to study the Falkner-Skan flow problem using the uniform Haar wavelet approach.

Organization of the paper is as follows: formulation of the two-dimensional boundary-layer flow over a moving wedge is given in Section 2. Section 3 devotes to give the details of Haar wavelets along with application of Haar wavelet to the problem in question. In Section 4, we illustrate the important findings in terms the velocity profiles, the wall shear stresses and effects of pressure gradient parameter on the flow. We summarize the important results of the work in Section 5. In the last Section 6 concluding remarks of the paper is reported.

2. FORMULATION

We consider a laminar boundary-layer flow of a viscous fluid over a moving wedge. The wedge is considered to be moving with velocity $U_w(x)$ opposite to the mainstream flow $U(x)$ (cf. Fig. 1). The cartesian coordinate system is employed in which x -axis measured along the direction of the mainstream flow (along the wedge surface) and y -axis is along normal to the flow; the flow occupies in the half space $y > 0$.

The fluid of a constant viscosity μ and density ρ is driven over a moving wedge with a large Reynolds number, $Re = \frac{UL}{\nu}$, where L is characteristic length of the wedge surface and ν is the kinematic viscosity. The large Reynolds number flow clearly divides the fluid into near-field and far-field regions. In the near-field region, the viscosity effects are considered to be significant. Once the boundary-layer is formed and if δ is the thickness of the boundary-layer, then we have $\delta \ll L$ and the thickness grows downstream of the wedge surface. As a consequence, we have $\frac{\partial u}{\partial x} \ll \frac{\partial u}{\partial y}$ and $\frac{\partial p}{\partial y} \ll \frac{\partial p}{\partial x}$. Accordingly, the pressure in the

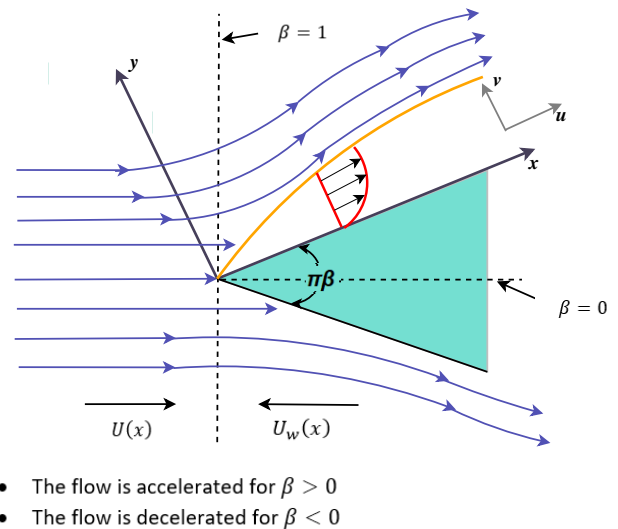


Fig. 1 Schematic diagram demonstrating the boundary-layer formation over a moving wedge.

boundary-layer has the same value as in the mainstream region. Thus, in the far-field region, the pressure is given by the Bernoulli's equation $-\frac{1}{\rho} \frac{dp}{dx} = U \frac{dU}{dx}$. Therefore, the Prandtl's boundary-layer equations which govern the laminar boundary-layer flow over a wedge are given by

$$\frac{\partial u}{\partial x} + \frac{\partial v}{\partial y} = 0 \quad (1)$$

$$u \frac{\partial u}{\partial x} + v \frac{\partial u}{\partial y} = U \frac{dU}{dx} + \nu \frac{\partial^2 u}{\partial y^2} \quad (2)$$

where u and v are velocity components in x and y directions. The relevant boundary conditions are

$$\begin{aligned} \text{at } y = 0 : \quad u &= U_w(x), \quad v = 0 \\ y \rightarrow \infty : \quad u &= U(x). \end{aligned} \quad (3)$$

From the boundary conditions, it is clear that, the velocity of the fluid varies from the velocity of the wedge on the surface to the velocity of the mainstream flow far-away from the surface. Further, both mainstream flow $U(x)$ and the wedge surface velocity $U_w(x)$ are approximated by the power of distance downstream of the boundary-layer, i.e.,

$$U(x) = U_\infty x^n \quad \text{and} \quad U_w(x) = U_0 x^n \quad (4)$$

where U_∞ and U_0 are non-negative constants and n is a constant that associates with the mainstream forcing on the boundary-layer. To solve the system (1)-(4), it is appropriate to use suitable similarity transformations on the assumption that the similar velocity profiles exist in the boundary-layer in x -direction. Introducing

$$\psi = \sqrt{\frac{2\nu x U}{1+n}} f(\eta), \quad \eta = \sqrt{\frac{(1+n)U}{2\nu x}} y \quad (5)$$

where the stream-function ψ is given by

$$(u, v) = \left(\frac{\partial \psi}{\partial y}, -\frac{\partial \psi}{\partial x} \right) \quad (6)$$

which satisfies the continuity Eq. (1) identically, into the momentum boundary-layer Eq. (2), we get

$$f'''(\eta) + f(\eta)f''(\eta) + \beta(1 - (f'(\eta))^2) = 0 \quad (7)$$

and the boundary conditions Eq. (3) becomes

$$f(0) = 0, \quad f'(0) = -\lambda, \quad f'(+\infty) = 1. \quad (8)$$

Here $\beta = \frac{2n}{n+1}$ in Eq. (7) represents the variable pressure gradient with $\beta > 0$, the flow is accelerated and $\beta < 0$, the flow is decelerated. For $\beta = 0$, the Blasius flow can be recovered. The parameter $\lambda = -\frac{U_0}{U_\infty}$ is the wedge velocity with $\lambda = 0$, the classical Falkner-Skan equation can be recovered. Although the system (7) and (8) is given in Sachdev *et al.* (2008), but it rederived here because complete details are not given. The Falkner-Skan Eqs. (7) and (8) is mathematically quite interesting because of nonlinearity and infinite domain and hence does not admit analytical solutions. Hartree (1937) gave numerical solution of the Falkner-Skan equation for $\lambda = 0$. Again for $\lambda = 0$, Weyl (1942) derived existence and uniqueness of the system (7) and (8). Later, Coppel (1960) proved the existence and uniqueness of the solutions on the basis that for non-zero $f(0)$ or $f'(0)$, $f''(\eta)$ is positive, zero or negative in the entire flow domain according to $f'(0)$ is less than, equal or greater than unity. In this paper, we follow quite different approach namely Haar wavelet analysis for the solution of non-linear differential equation given in Eqs. (7)-(8). Various properties, domain conversion, etc. are discussed with respect to the system (7)-(8). Various details of the Haar wavelet are given in the following section. We use two different Haar wavelet approaches with and without quasilinearization technique. This is followed by the residual and error estimates in both cases.

3. HAAR WAVELETS

Several fine properties of Haar wavelets would certainly lead to an efficient numerical method for differential equations. The Haar wavelets are most simple among different wavelet families with explicit expression for scaling and wavelet functions. In 1910, Alfred Haar introduced the Haar function as a group of square waves with magnitude ± 1 in some finite intervals and vanishes outside of the interval, which are orthonormal and locally supported. These properties minimize the calculation process and simplifies the solution procedure. The wavelet bases are generally constructed by means of multiresolution analysis (Daubechies (1992)). For the purpose of the current problem, it will suffice to say that the Haar scaling function $h_1(t)$ is defined by

$$h_1(t) = \begin{cases} 1, & t \in [0, 1) \\ 0, & \text{elsewhere.} \end{cases}$$

The Haar mother wavelet is obtained as the linear combination of the Haar scaling function:

$$h_2(t) = h_1(2t) - h_1(2t - 1). \quad (9)$$

All the other subsequent wavelets are generated from dilations and translations of mother wavelet. This can be expressed in a more compact form as follows:

$$h_i(t) = \begin{cases} h_2(2^j t - k) \\ = \begin{cases} 1, & t \in [a, b) \\ -1, & t \in [b, c) \\ 0, & \text{elsewhere} \end{cases} \end{cases} \quad (10)$$

where

$$a = \frac{k}{m}, \quad b = \frac{k+0.5}{m}, \quad c = \frac{k+1}{m}.$$

The translation parameter $k = 0, 1, \dots, m - 1$ ($m = 2^j$) determines location of wavelet, $j = 0, 1, \dots, J$; the dilation parameter which measures degree of compression, J is the level of resolution and $i = m+k+1$ is the wavelet number. Notice that all the Haar wavelets are orthogonal to each other. That is,

$$\int_0^1 h_r(t)h_s(t)dt = \begin{cases} 2^{-j}, & r = s \\ 0, & r \neq s. \end{cases} \quad (11)$$

Evidently, $\{h_i(t)\}$ defined in Eq. (10) form an orthogonal wavelet bases for $L^2[0, 1)$. Thus, any function $g(t) \in L^2[0, 1)$ can be decomposed as

$$g(t) = \sum_{i=1}^{\infty} a_i h_i(t), \quad t \in [0, 1) \quad (12)$$

where a_i are the Haar wavelet coefficients and are calculated as $a_i = \langle h_i(t), g(t) \rangle$. Furthermore, if $g(t)$ is a piecewise constant or possibly approximated as piecewise constants, then the series expansion of $g(t)$ in Eq. (12) will be terminated after finite terms. Integration of the Haar functions in Eq. (10) can be expressed as

$$p_{1,i}(t) = \int_0^t h_i(x)dx \quad (13)$$

and subsequent integration can be recursively defined as

$$p_{\alpha,i}(t) = \int_0^t p_{\alpha-1,i}(x)dx, \quad \alpha = 2, 3, \dots$$

$$= \begin{cases} 0 & \text{for } t \in [0, a), \\ \frac{1}{\alpha!} [t-a]^\alpha & \text{for } t \in [a, b), \\ \frac{1}{\alpha!} \{ [t-a]^\alpha - 2[t-b]^\alpha \} & \text{for } t \in [b, c), \\ \frac{1}{\alpha!} \{ [t-a]^\alpha - 2[t-b]^\alpha + [t-c]^\alpha \} & \text{for } t \in [c, 1) \end{cases} \quad (14)$$

where $i = 2, 3, \dots, 2^{J+1}$. For $i = 1$, we have

$$p_{\alpha,1}(t) = \frac{t^\alpha}{\alpha!}, \quad \alpha = 1, 2, 3, \dots \quad (15)$$

The sparsity pattern of Haar matrix $h_i(t)$ and its first integral $p_{1,i}(t)$

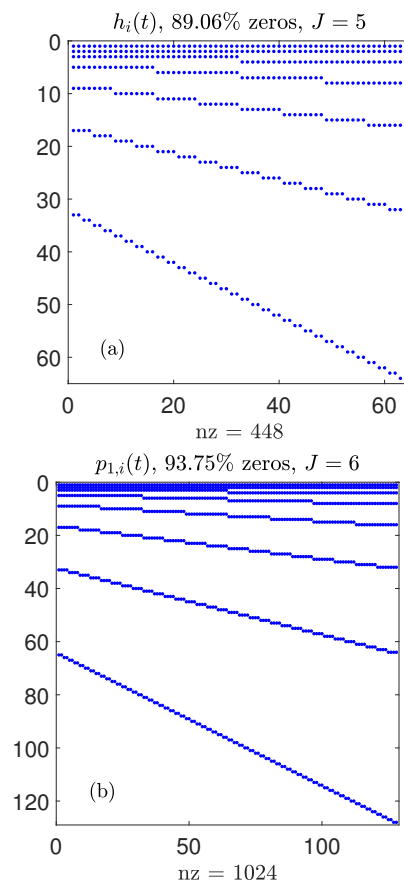


Fig. 2 Nonzero structure of Haar matrix $h_i(t)$ and its first integral $p_{1,i}(t)$.

are shown in Fig. 2 for $J = 5$ and $J = 6$ respectively. We notice that as the size of the matrices increases (i.e., J increases), the sparsity of the matrices also increases which is very convenient for computer implementations.

4. METHOD OF SOLUTION

We convert the semi-infinite interval of Eq. (7) with relevant boundary conditions Eq. (8) to Haar wavelet environment by replacing the third boundary condition in Eq. (8) with the condition

$$f'(\eta_\infty) = 1 \quad (16)$$

for some 'sufficiently large' value η_∞ of η which varies with β and λ and is determined by introducing an asymptotic condition

$$f''(\eta_\infty) = 0. \quad (17)$$

Normalizing the Eqs. (7)-(8) by the coordinate transformation $\xi = \eta/\eta_\infty$ and the change of variable $F(\xi) = f(\eta)/\eta_\infty$, ensuring that all the boundary conditions Eq. (8) are satisfied. This reduces Eq. (7) to the form

$$F'''(\xi) + \eta_\infty^2 F(\xi)F''(\xi) + \eta_\infty^2 \beta (1 - (F'(\xi))^2) = 0. \quad (18)$$

Accordingly, the conditions Eq. (8) are transformed to

$$F(0) = 0, \quad F'(0) = -\lambda, \quad F'(1) = 1. \quad (19)$$

The boundary value problem Eqs. (7) and (8) defined over an infinite domain is now converted into [0,1) (cf. Eqs. (8) and (19)).

4.1. Haar wavelet quasilinearization method (HWQLM)

In this method, we apply the concept of quasilinearization technique introduced by Bellman and Kalaba (1965), which is a generalization of the Newton-Raphson method in function space, to linearize the non-linear terms $F(\xi)F''(\xi)$ and $(F'(\xi))^2$ in Eq. (18). It converges quadratically to the exact solution (Mandelzweig and Tabakin (2001)) and the convergence rate depends on the initial guess of the solution. The linearized form of Eq. (18) is

$$F_{r+1}'''(\xi) + \eta_\infty^2 F_r(\xi)F_{r+1}''(\xi) - 2\eta_\infty^2 \beta F_r'(\xi)F_{r+1}'(\xi) + \eta_\infty^2 F_r''(\xi)F_{r+1}(\xi) = \eta_\infty^2 F_r(\xi)F_r''(\xi) - \eta_\infty^2 \beta (F_r'(\xi))^2 - \eta_\infty^2 \beta \quad (20)$$

with corresponding boundary conditions

$$F_{r+1}(0) = 0, \quad F_{r+1}'(0) = -\lambda, \quad F_{r+1}'(1) = 1. \quad (21)$$

The subscript r denotes the known quantity which is used to obtain the unknown quantities denoted by subscript $r + 1$ through iterative process. We shall develop the highest derivative in Eq. (20) into the Haar wavelet series (see Chen and Hsiao (1997)) and on successively integrating, the derivatives of lower order and the solution functions are evaluated as follows:

$$F_{r+1}'''(\xi) = \sum_{i=1}^{2^{J+1}} a_i h_i(\xi) \quad (22)$$

$$F_{r+1}''(\xi) = \sum_{i=1}^{2^{J+1}} a_i [p_{1,i}(\xi) - C_i] + 1 + \lambda \quad (23)$$

$$F_{r+1}'(\xi) = \sum_{i=1}^{2^{J+1}} a_i [p_{2,i}(\xi) - \xi C_i] - \lambda + \xi(1 + \lambda) \quad (24)$$

$$F_{r+1}(\xi) = \sum_{i=1}^{2^{J+1}} a_i \left[p_{3,i}(\xi) - \frac{\xi^2}{2} C_i \right] - \lambda \xi + \frac{\xi^2}{2} (1 + \lambda) \quad (25)$$

where

$$C_i = \int_0^1 p_{1,i}(t) dt. \quad (26)$$

Substituting Eqs. (22)-(25) in Eq. (20), we attain a system of 2^{J+1} number of algebraic equations with 2^{J+1} unknown wavelet coefficients a_i .

We use collocation method for calculating a_i . The collocation points are defined as

$$\xi_l = \frac{1}{2^{J+1}} \left(l - \frac{1}{2} \right), \quad l = 1, 2, \dots, 2^{J+1}. \quad (27)$$

Consequently, the discrete form of Eq. (20) after replacing it into Eqs. (22)-(25) is

$$\sum_{i=1}^{2^{J+1}} a_i \left[H(i, l) + \eta_\infty^2 F_r(\xi_l) P1(i, l) - \eta_\infty^2 F_r(\xi_l) C - 2\eta_\infty^2 \beta F_r'(\xi_l) P2(i, l) + 2\eta_\infty^2 \beta \xi_l F_r'(\xi_l) C + \eta_\infty^2 F_r''(\xi_l) P3(i, l) - \frac{\eta_\infty^2}{2} \xi_l^2 F_r''(\xi_l) C \right] = \eta_\infty^2 F_r(\xi_l) F_r''(\xi_l) - \eta_\infty^2 \beta (F_r'(\xi_l))^2 - \eta_\infty^2 \beta - \eta_\infty^2 F_r(\xi_l) - \lambda \eta_\infty^2 F_r(\xi_l) - 2\eta_\infty^2 \beta \lambda F_r'(\xi_l) + 2\eta_\infty^2 \beta \xi_l F_r'(\xi_l) + 2\eta_\infty^2 \beta \lambda \xi_l F_r'(\xi_l) + \eta_\infty^2 \lambda \xi_l F_r''(\xi_l) - \eta_\infty^2 \frac{\xi_l^2}{2} F_r''(\xi_l) - \eta_\infty^2 \lambda \frac{\xi_l^2}{2} F_r''(\xi_l) \quad (28)$$

or more conveniently in compact form

$$\mathbf{A} \mathbf{X} = \mathbf{B} \quad (29)$$

where $\mathbf{A} = (a_i)$ is a 2^{J+1} dimensional row vector, $H(i, l) = h_i(\xi_l)$ is the element of a $2^{J+1} \times 2^{J+1}$ matrix, $P_r(i, l) = p_{r,i}(\xi_l)$, $r = 1, 2, 3$ are integral matrices defined as in Section 3, $C = (C_i)$ is a 2^{J+1} dimensional column vector given by Eq. (26), \mathbf{X} and \mathbf{B} are respectively the expressions inside the square bracket and right side of Eq. (28). With a suitable initial approximation, the system Eq. (29) is solved for Haar coefficients. The computations were accomplished with the aid of the MATLAB programs, which is very efficient in matrix representation.

4.2. Haar wavelet method (HWM)

The non-linear differential equation Eq. (18) with pertinent boundary conditions Eq. (19) is also solved directly using Haar wavelets with collocation method without quasilinearization. In this method, we seek the Haar wavelet approximation of $F'''(\xi)$ in Eq. (18) in the form Eq. (22) and apply the Haar wavelet method described in Section 4.1. Accordingly, Eq. (18) simplifies to a system of 2^{J+1} nonlinear equations, which is put into discrete form by making use of collocation points Eq. (27) as

$$\mathbf{F}_l(\xi_l, \mathbf{A}) = 0. \quad (30)$$

That is,

$$\sum_{i=1}^{2^{J+1}} a_i H(i, l) + \eta_\infty^2 \left[\sum_{i=1}^{2^{J+1}} a_i P3(i, l) + \frac{\xi_l^2}{2} (1 + \lambda) - \frac{\xi_l^2}{2} \sum_{i=1}^{2^{J+1}} a_i C - \lambda \xi_l \right] \left[\sum_{i=1}^{2^{J+1}} a_i P1(i, l) + 1 + \lambda - \sum_{i=1}^{2^{J+1}} a_i C \right] + \eta_\infty^2 \beta \left[1 - \left(\sum_{i=1}^{2^{J+1}} a_i P2(i, l) + \xi_l (1 + \lambda) - \xi_l \sum_{i=1}^{2^{J+1}} a_i C - \lambda \right)^2 \right] = 0. \quad (31)$$

Newton's method is applied for solving Eq. (31) to compute the wavelet coefficients:

$$\mathbf{A} \leftarrow \mathbf{A} + \Delta \mathbf{A} \quad (32)$$

where $\Delta \mathbf{A}$ satisfies the equation

$$\mathbf{S}(i, l) \Delta \mathbf{A} = -\mathbf{F}_l \quad (33)$$

and

$$\mathbf{S}(i, l) = \frac{\partial \mathbf{F}_l}{\partial a_i}. \quad (34)$$

This process is repeated recursively until the difference between two consecutive iterates is less than or equal to 10^{-12} . The shear stress at the wall is evaluated as

$$f''(0) = \frac{1}{\eta_\infty} [(1 + \lambda)D - \mathbf{AC}] \quad (35)$$

where D is a 2^{J+1} row vector of ones. Our MATLAB program is developed to find the wavelet solution. The computer simulations are performed for numerous values of β and λ , and the results will be discussed later.

4.3. Residual and Error Estimates

It is observed that for Haar wavelet approximation, the error is inversely proportional to the level of resolution. The convergence rate for the Haar wavelet series is $\mathbf{O}[(\frac{1}{2^{J+1}})^2]$, since it belongs to the set of piecewise constant functions (Majak *et al.* (2015)). However, we measure the degree of exactness of the Haar approximations to the governing problem Eq. (7) by evaluating the residual and error estimation, which are given by the following respective relations: the residual of Eq. (7) defined as

$$\sigma_{\text{res}} = \|\varepsilon(\eta_l)\|/2^{J+1} \quad (36)$$

where

$$\varepsilon(\eta_l) = f'''(\eta_l) + f(\eta_l)f''(\eta_l) + \beta(1 - (f'(\eta_l))^2). \quad (37)$$

The solution error of Eq. (7) defined as

$$\sigma_{\text{err}} = \|\Delta_J(\eta_l)\|/2^{J+1} \quad (38)$$

where

$$\Delta_J(\eta_l) = f_J(\eta_l) - f_{J+1}(\eta_l) \quad (39)$$

and $f_J(\eta)$ and $f_{J+1}(\eta)$ are solutions of Eq. (7) for resolution levels J and $J + 1$ respectively, $\eta_l, l = 1, 2, \dots, 2^{J+1}$ are the collocation points at resolution level J .

5. RESULTS AND DISCUSSION

Haar wavelet and Haar wavelet quasilinearization methods have been developed for the two-dimensional boundary-layer flow over a moving wedge modelled by the Falkner-Skan equation. These methods depend on the different resolution levels J in which for large J both error and residual tend to zero. However, for given J , we use collocation method to determine 2^{J+1} unknown wavelet coefficients in the system. In both cases, matrix inversion is required for which the MATLAB is used. To this end, the profiles and the wall-shear stresses have been computed for various values of physical parameters β and λ . Once the required solutions are obtained in $[0, 1)$, we revert back to η (defined over $[0, \infty)$) from ξ . The physical characteristics are discussed in terms of η . Haar wavelet simulations for both accelerated and decelerated flows are obtained.

Table 1 Error estimates for Eq. (7) using HWQLM for $\beta = 0.5, 1.5$ and different resolution level J .

J	σ_{err} for $\beta = 0.5$		σ_{err} for $\beta = 1.5$	
	$\lambda = -1.1$	$\lambda = -1.5$	$\lambda = -1.1$	$\lambda = -1.5$
4	6.9249E-06	4.0939E-05	6.8590E-06	4.0817E-05
5	1.2208E-06	7.2134E-06	1.2169E-06	7.2592E-06
6	2.1567E-07	1.2741E-06	2.1531E-07	1.2852E-06
7	3.8118E-08	2.2519E-07	3.8071E-08	2.2728E-07
8	6.7382E-09	3.9806E-08	6.7304E-09	4.0182E-08
9	1.1911E-09	7.0367E-09	1.1898E-09	7.1034E-09

Before starting any physical aspect, we discuss robustness and efficiency of the HWQLM and HWM in terms of estimation of errors and residual. These are estimated for two sets of λ and for $\beta = 0.5$ and

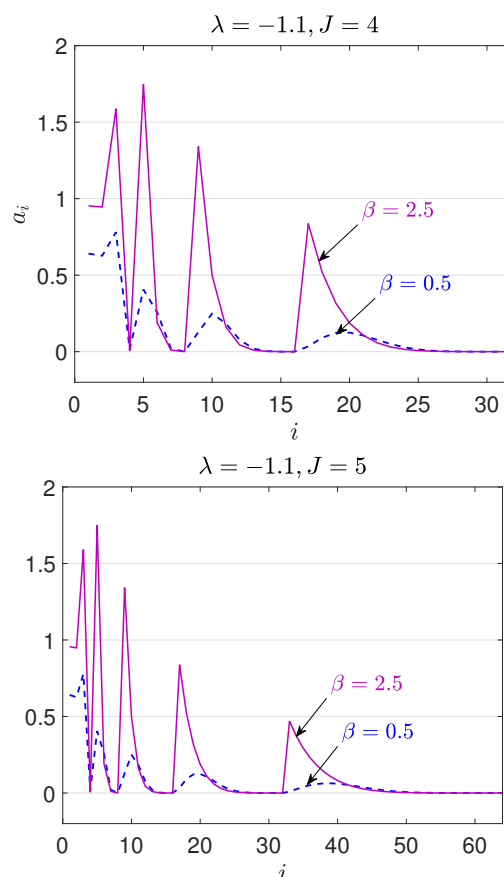


Fig. 3 Haar wavelet coefficients.

1.5 for different resolution levels. Table 1 clearly addresses that the error estimate σ_{err} decreases gradually for increasing J . In this case, the determinant $|\mathbf{X}|$ increases exponentially for increasing J which provides a favourable situation for accurate calculation of the Haar coefficients a_i (i.e. $|\mathbf{X}|$ for $\beta = 1.5$ and $\lambda = 1.1$ at various resolution levels $J = 4, 5, 6, 7, 8$ are respectively $4.94E + 11, 2.65E + 21, 5.53E + 40, 2.00E + 79, 2.40E + 156$). Some of these Haar wavelet coefficients a_i presented in Fig. 3 for $\beta = 0.5$ and for two different resolution levels. It is noticed that, increase in the wavelet number i results in fast decrease of the wavelet coefficients a_i . This ability to accurately represent solution functions with a small number of adaptively chosen wavelet coefficients makes one of the main attractive features of our proposed method. The same trend is preserved even for $\beta = 2.5$ in the same figure. Furthermore, the variation of the residual estimate σ_{res} as a function of J is depicted in Fig. 4 for $\lambda = -1.1, -1.5$ and for $\beta = 0.5$. We observe that there is a direct relation between solution error and residual. Note that the error decreases as residual becomes smaller and smaller, and the residual σ_{res} decreases for increasing J .

Table 2 compares the present HWQLM and HWM results for the velocity profiles $f'(\eta)$ at various η values with those produced by Sachdev *et al.* (2008) for two sets of β and for $\lambda = -1.4$. It is clearly observed that our present solutions are in excellent agreement up to desired accuracy. To compute these results the resolution level J was set to 10 where the error estimate is very much small. We intentionally simulated the same results for $\lambda = -1.1, -1.3$, etc., (though not shown in Table 2), but there is no change in the accuracy. Our computational code always begins at the resolution level $J = 1$ and depends on the tolerance which is set to 10^{-12} in all the simulations.

On the other hand, we now turn our attention to discuss the various solutions such as $f(\eta), f'(\eta)$ and $f''(\eta)$ that are obtained from both

Table 2 Comparison of Haar wavelet solutions $f'(\eta)$ of Eq. (7) with those obtained by HWQLM and exact solutions for $\lambda = -1.4$ ($J = 10$).

η	$\beta = 0$			$\beta = 1.0$		
	HWQLM	HWM	Sachdev et al. (2008)	HWQLM	HWM	Sachdev et al. (2008)
0.00	1.4	1.4	1.4	1.4	1.4	1.4
0.25	1.31193175	1.31193175	1.31193075	1.25571272	1.25571272	1.25571373
0.50	1.23093573	1.23093573	1.23093380	1.15748961	1.15748961	1.15749169
0.75	1.16210173	1.16210173	1.16209902	1.09322033	1.09322033	1.09322362
1.00	1.10779722	1.10779722	1.10779390	1.05291736	1.05291736	1.05292200
1.25	1.06787539	1.06787539	1.06787159	1.02875319	1.02875319	1.02875938
1.50	1.04044746	1.04044746	1.04044332	1.01492908	1.01492908	1.01493703
1.75	1.02279959	1.02279959	1.02279520	1.00739558	1.00739558	1.00740543
2.00	1.01215034	1.01215034	1.01214562	1.00349057	1.00349057	1.00350180
2.25	1.00611838	1.00611838	1.00611267	1.00156760	1.00156760	1.00157495
2.50	1.00290960	1.00290960	1.00290023	1.00066896	1.00066896	1.00064411
2.75	1.00130602	1.00130602	1.00128485	1.00027079	1.00027079	1.00011411
3.00	1.00055306	1.00055306	1.00049991	1.00010364	1.00010364	1.00005186
3.25	1.00022084	1.00022084	1.00009325	1.00003717	1.00003717	1.00000617
3.50	1.00008311	1.00008311	-	1.00001211	1.00001211	-
3.75	1.00002944	1.00002944	-	1.00000312	1.00000312	-
4.00	1.00000980	1.00000980	-	1.00000000	1.00000000	-

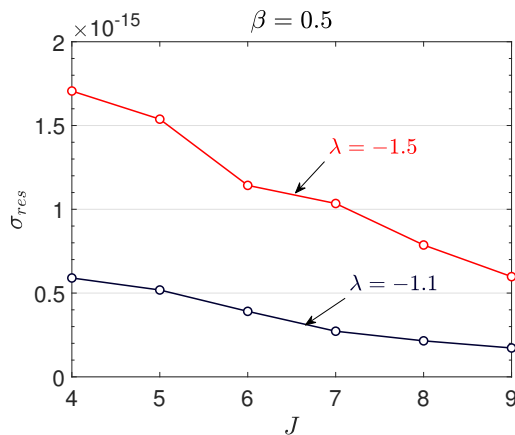


Fig. 4 Estimation of residual, σ_{res} versus level of resolution.

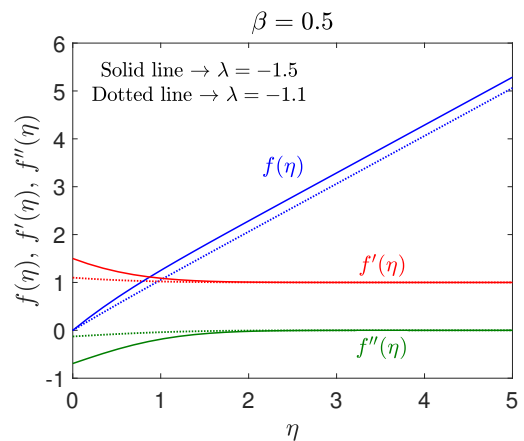


Fig. 5 Haar wavelet solution for $\beta = 0.5$ and $\lambda = -1.1, -1.5$.

methods discussed above. Figure 5 discusses various solutions for two values of λ . The solution $f(\eta)$ approaches to infinity as $\eta \rightarrow \infty$ whereas $f'(\eta)$ tends to its asymptotic value unity as $\eta \rightarrow \infty$ (cf. Eq. (8)). Also $f''(\eta)$ approaches zero from below. Thus, these solutions confirm an exact fluid dynamics of the problem, for example, the last derivative boundary condition $f'(\eta) \rightarrow 1$ as $\eta \rightarrow \infty$ suggests that $f(\eta) \rightarrow \eta \rightarrow \eta_0$, as $\eta \rightarrow \infty$, where η_0 is an integration constant (however $\eta_0 = 0$, in the present problem). This shows the accuracy and efficiency of the proposed scheme. The similar trends are observed for any choice of λ and β though not shown here. Also, we particularly plot the velocity profiles as a functions of η in Fig. 6 for various accelerated pressure gradient parameter β . Nevertheless, the effects of pressure gradients on the boundary-layer flow are given in Fig. 6. Note that thickness of the boundary-layer decreases as β increases, and profiles approach the mainstream flow rapidly for strong accelerated flows. Figure 6 shows the variation of the velocity profiles $f'(\eta)$ with η for various values of λ for two sets of β . It is clearly noticed that profiles approach the mainstream flow almost in the same speed. These profiles have been drawn using the HWQLM since both approaches give the same solutions.

Surprisingly, the HWM for the Falkner-Skan equation predicts multiple solutions depending on the values of β and are shown in Fig. 8. These results are shown in terms of the wall shear stress $f''(0)$ in the figure. Note that for $\lambda < 0$, the method predicts only a single solution for

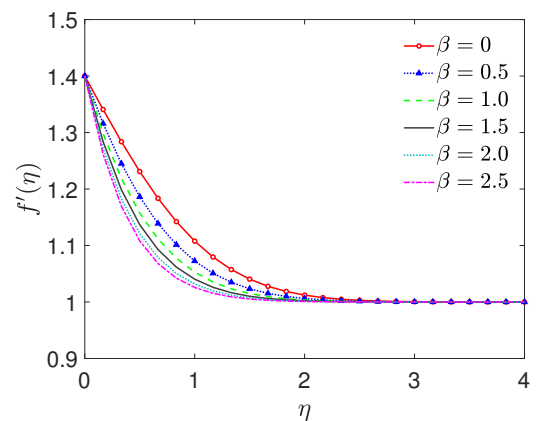


Fig. 6 Variation of velocity $f'(\eta)$ with η for different values of β with $\lambda = -1.4$.

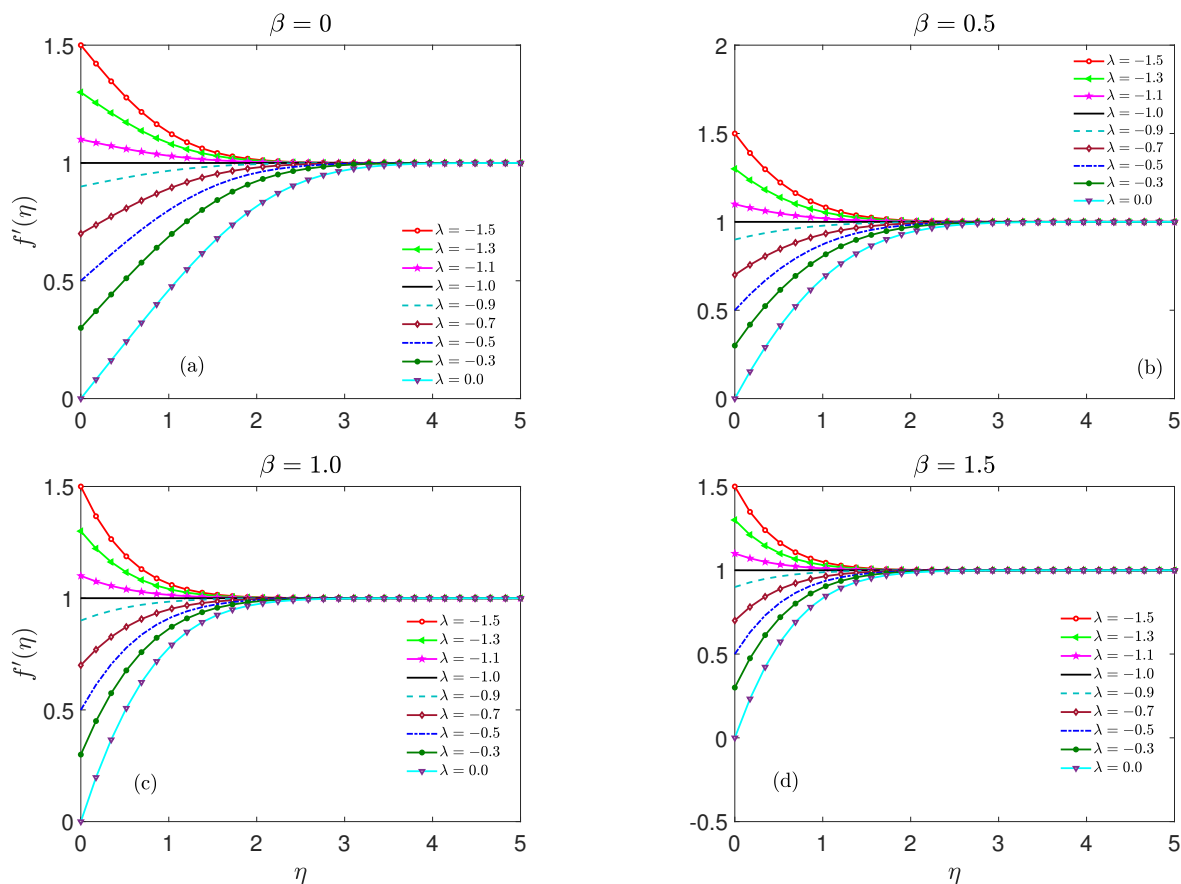


Fig. 7 Velocity profiles in the boundary layers under different values of β .

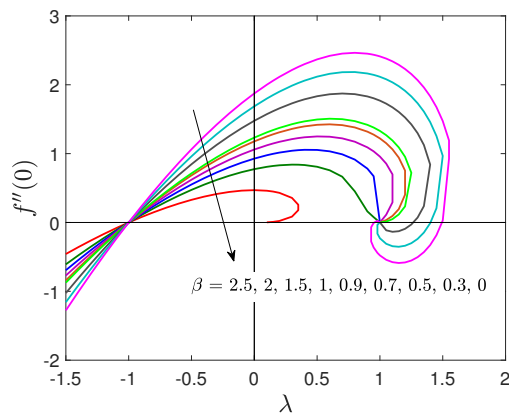


Fig. 8 The wall shear stresses $f''(0)$ versus λ for various β .

all β . At $\lambda = -1$, the wall shear stress vanishes for all β which means that there is exact and trivial solution $f(\eta) = \eta$ for Eqs. (7) and (8) which satisfies all the boundary conditions (Sachdev *et al.* (2008)). Note that for $\beta \in (0, 0.5]$, only one solution is available for the Falkner-Skan equation. In fact, there is unique solution for all $\lambda \lesssim 0.9$. There are dual solutions for the system in the range $\beta \in (0.5, 1]$ for $\lambda > 1$. In fact the system also predicts the triple solutions for $\beta > 1$. Exceptionally, the case $\beta = 0$ also predicts dual solutions. We note here that these multiple solutions are obtained by setting η_∞ value quite large (> 10) for every other solution. Merchant and Davis (1989) have shown that no solution is available for $\lambda \gtrsim 1.6$.

In order to assess the nature of these multiple solutions, we intentionally plot the velocity profiles for selected values of λ and β and are shown in Fig. 9 for dual solutions and in Fig. 10 for triple solutions. As shown in Figs. 6 and 7, every first solution in Figs. 9 and 10 approach the end-boundary condition rapidly whereas the second and third solutions take quite larger boundary-layer domain to the mainstream flows which is seen in these figures.

6. CONCLUSION

In the present paper, the Falkner-Skan equation representing the boundary-layer flow of a viscous fluid over a moving wedge is reinvestigated by proposing two new composite numerical methods based on uniform Haar wavelets combined with quasilinearization and collocation approach. The main benefits of our proposed method are its simplicity, reliability, and cost-effectiveness. Due to several inherent features of Haar wavelets, such as sparsity of the transform matrix, small number of wavelet coefficients, etc., the proposed method provides excellent results for the involved pertinent parameters. It is worth mentioning that the Haar wavelet method effectively unfolds the existence and multiplicity of solutions of

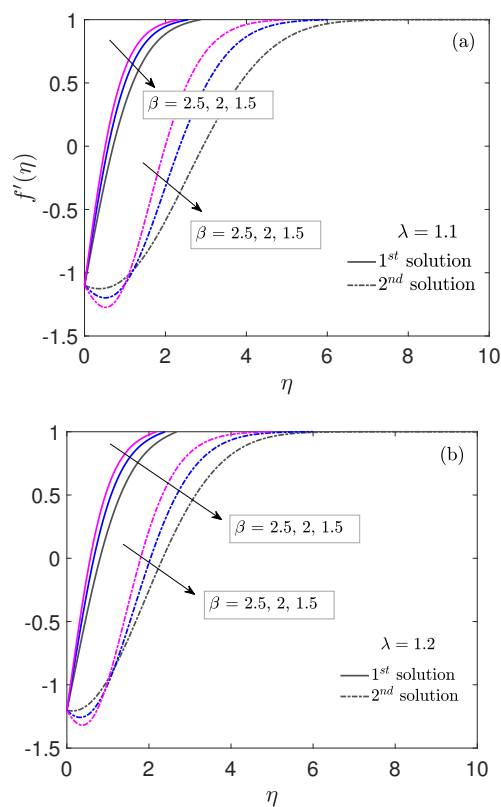


Fig. 9 Variation of velocity $f'(\eta)$ with η for dual solutions at (a) $\lambda = 1.1$ and (b) $\lambda = 1.2$.

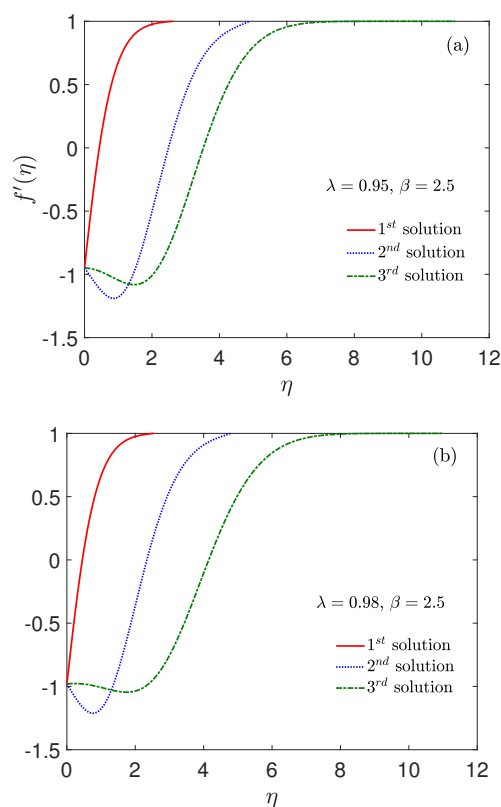


Fig. 10 Variation of velocity $f'(\eta)$ with η for triple solutions at (a) $\lambda = 0.95$ and (b) $\lambda = 0.98$.

the governed problems for different derived quantities and provides accurate results with less computational cost. This method can be easily extended to solve many other nonlinear boundary value problems of fluid mechanics and plays a convenient alternate over other numerical and semi-analytical methods. Also, the proposed scheme is more suitable for the numerical solution of boundary value problems defined on long intervals.

NOMENCLATURE

x, y	coordinates of Cartesian system of axes (m)
u, v	flow velocities in the x and y directions respectively (m/s)
ν, ρ	kinematic viscosity (m^2/s) and the fluid density (kg/m^3) respectively
L	length of the wedge surface (m)
δ	thickness of the boundary-layer (m)
Re	Reynolds number
$U_w(x)$	wedge surface velocity (m/s)
$U(x)$	mainstream flow velocity (m/s)
U_∞, U_0	non-negative constants associated with mainstream flow and wedge surface flow respectively
β	variable pressure gradient, dimensionless
ψ	stream function (m^2/s)
η	non-dimensional variable
$f(\eta)$	non-dimensional function related to the stream function
$f''(0)$	wall shear stress
i	wavelet number
j	dilation parameter
k	translation parameter
J	resolution level
$h_i(t)$	Haar wavelet function
$P_{\alpha,i}(t)$	subsequent integration of Haar wavelet function
a_i	Haar coefficients, dimensionless
$\sigma_{res}, \sigma_{err}$	residual and solution error estimates respectively

REFERENCES

Abdelmeguid, M.S., 2017, "Hydromagnetic Viscous Fluid over a Non-linear Stretching and Shrinking Sheet in the Presence of Thermal Radiation," *Frontiers in Heat and Mass Transfer*, **8**(28), 1–8. <http://dx.doi.org/10.5098/hmt.8.28>.

Ariel, P.D., 2007, "The Three-dimensional Flow Past a Stretching Sheet and the Homotopy Perturbation Method," *Computers & Mathematics with Applications*, **54**(7), 920–925. <https://doi.org/10.1016/j.camwa.2006.12.066>.

Ariel, P., 1994, "MHD Flow of a Viscoelastic Fluid Past a Stretching Sheet with Suction," *Acta Mechanica*, **105**(1), 49–56. <https://doi.org/10.1007/BF01183941>.

Bellman, R., and Kalaba, R., 1965, *Quasilinearization and Nonlinear Boundary-Value Problems*, American Elsevier Publishing Company. <https://www.rand.org/pubs/reports/R438.html>.

Bhattacharyya, K., 2012, "Slip Effects on Boundary Layer Flow and Mass Transfer with Chemical Reaction Over a Permeable Flat Plate in a Porous Medium," *Frontiers in Heat and Mass Transfer*, **3**(043006), 1–6. <http://dx.doi.org/10.5098/hmt.v3.4.3006>.

Chen, C., and Hsiao, C., 1997, "Haar Wavelet Method for Solving Lumped and Distributed-Parameter Systems," *IEE Proc-Control Theory Appl*, **144**(1), 87–94. <https://doi.org/10.1049/ip-cta:19970702>.

- Coppel, W., 1960, "On a Differential Equation of Boundary-Layer Theory," *Philosophical Transactions of the Royal Society of London Series A*, **253**, 101–136. <https://doi.org/10.1098/rsta.1960.0019>.
- Daubechies, I., 1992, *Ten Lectures on Wavelets*, Society for Industrial and Applied Mathematics. <https://doi.org/10.1137/1.9781611970104>.
- Erfanian, M., Gachpazan, M., and Beiglo, H., 2017, "A New Sequential Approach for Solving the Integro-differential Equation via Haar Wavelet Bases," *Computational Mathematics and Mathematical Physics*, **57**(2), 297–305. <https://doi.org/10.1134/S096554251702004X>.
- Ganapathirao, M., Chamkha, A.J., and Rao, N.S., 2019, "Effects of Non-uniform Slot Suction/injection and Chemical Reaction on Mixed Convective MHD Flow along a Vertical Wedge Embedded in a Porous Medium," *Frontiers in Heat and Mass Transfer*, **13**(15), 1–13. <http://dx.doi.org/10.5098/hmt.13.15>.
- Govindaraj, N., Singh, A.K., and Shukla, P., 2020, "Fluid Flow and Heat Transfer Over a Stretching Sheet with Temperature Dependent Prandtl Number and Viscosity," *Frontiers in Heat and Mass Transfer*, **15**(20), 1–8. <http://dx.doi.org/10.5098/hmt.15.20>.
- Hartree, D., 1937, "On an Equation Occurring in Falkner and Skan's Approximate Treatment of the Equations of the Boundary Layer," *Mathematical Proceedings of the Cambridge Philosophical Society*, **33**, 223–239. <https://doi.org/10.1017/S0305004100019575>.
- Ishak, A., Nazar, R., and Pop, I., 2007, "MHD Boundary-layer Flow due to a Moving Extensible Surface," *Journal of Engineering Mathematics*, **62**(1), 23–33. <https://doi.org/10.1007/s10665-007-9169-z>.
- Jiwari, R., 2015, "A Hybrid Numerical Scheme for the Numerical Solution of the Burgers' Equation," *Computer Physics Communications*, **188**, 59–67. <https://doi.org/10.1016/j.cpc.2014.11.004>.
- Kaur, H., Mittal, R., and Mishra, V., 2011, "Haar Wavelet Quasilinearization Approach for Solving Nonlinear Boundary Value Problems," *American Journal of Computational Mathematics*, **1**, 176–182. <https://doi.org/10.4236/ajcm.2011.13020>.
- Kaur, H., Mittal, R., and Mishra, V., 2014, "Haar Wavelet Solutions of Nonlinear Oscillator Equations," *Applied Mathematical Modelling*, **38**(21), 4958–4971. <https://doi.org/10.1016/j.apm.2014.03.019>.
- Kumaresan, E., and Kumar, A.G.V., 2017, "An Exact Solution on Unsteady MHD Viscoelastic Fluid Flow Past an Infinite Vertical Plate in the Presence of Thermal Radiation," *Frontiers in Heat and Mass Transfer*, **8**(9), 1–7. <http://dx.doi.org/10.5098/hmt.8.9>.
- Lepik, Ü., 2005, "Numerical Solution of Differential Equations Using Haar Wavelets," *Mathematics and Computers in Simulation*, **68**(2), 127–143. <https://doi.org/10.1016/j.matcom.2004.10.005>.
- Lepik, Ü., 2006, "Haar Wavelet Method for Nonlinear Integro-differential Equations," *Applied Mathematics and Computation*, **176**(1), 324–333. <https://doi.org/10.1016/j.amc.2005.09.021>.
- Lepik, Ü., 2008, "Haar Wavelet Method for Solving Higher Order Differential Equations," *International Journal of Mathematics and Computation*, **1**(N08), 84–94. <http://www.ceser.in/ceserp/index.php/ijmc/article/view/2380>.
- Liao, S.J., 1999, "A Uniformly Valid Analytic Solution of Two-dimensional Viscous Flow over a Semi-infinite Flat Plate," *Journal of Fluid Mechanics*, **385**, 101–128. <https://doi.org/10.1017/S0022112099004292>.
- Majak, J., Pohlak, M., Karjust, K., Eerme, M., Kurnitski, J., and Shvartsman, B.S., 2018, "New higher order Haar wavelet method: Application to FGM structures," *Composite Structures*, **201**, 72–78. <https://doi.org/10.1016/j.compstruct.2018.06.013>.
- Majak, J., Shvartsman, B., Kirs, M., Pohlak, M., and Herranen, H., 2015, "Convergence Theorem for the Haar Wavelet Based Discretization Method," *Composite Structures*, **126**, 227–232. <https://doi.org/10.1016/j.compstruct.2015.02.050>.
- Mandelzweig, V., and Tabakin, F., 2001, "Quasilinearization Approach to Nonlinear Problems in Physics with Application to Nonlinear ODEs," *Computer Physics Communications*, **141**(2), 268–281. [https://doi.org/10.1016/S0010-4655\(01\)00415-5](https://doi.org/10.1016/S0010-4655(01)00415-5).
- Mansoori, M., and Nazemi, A., 2016, "Solving Infinite-horizon Optimal Control Problems of the Time-delayed Systems by Haar Wavelet Collocation Method," *Computational and Applied Mathematics*, **35**(1), 97–117. <https://doi.org/10.1007/s40314-014-0184-1>.
- Mehrpourvar, M., Majak, J., Karjust, K., and Arda, M., 2022, "Free vibration analysis of tapered Timoshenko beam with higher order Haar wavelet method," *Proceedings of the Estonian Academy of Sciences*, **71**(1), 77–83. <https://doi.org/10.3176/proc.2022.1.07>.
- Merchant, G.J., and Davis, S.H., 1989, "Modulated Stagnation Point Flow and Steady Streaming," *Journal of Fluid Mechanics*, **198**, 543–555. <https://doi.org/10.1017/S0022112089000248>.
- Mittal, R., and Pandit, S., 2017, "Numerical Simulation of Unsteady Squeezing Nanofluid and Heat Flow Between Two Parallel Plates Using Wavelets," *International Journal of Thermal Sciences*, **118**, 410–422. <https://doi.org/10.1016/j.ijthermalsci.2017.04.019>.
- Rashidi, M., and Erfani, E., 2011, "The Modified Differential Transform Method for Investigating Nano Boundary-layers over Stretching Surfaces," *International Journal of Numerical Methods for Heat & Fluid Flow*, **21**(7), 864–883. <https://doi.org/10.1108/09615531111162837>.
- Ratas, M., Majak, J., and Salupere, A., 2021a, "Solving Nonlinear Boundary Value Problems Using the Higher Order Haar Wavelet Method," *Mathematics*, **9**(21), 1–12. <https://doi.org/10.3390/math9212809>.
- Ratas, M., Salupere, A., and Majak, J., 2021b, "Solving Nonlinear PDEs Using the Higher Order Haar Wavelet Method on Nonuniform and Adaptive Grids," *Mathematical Modelling and Analysis*, **26**(1), 147–169. <https://doi.org/10.3846/mma.2021.12920>.
- Riley, N., and Weidman, P.D., 1989, "Multiple Solutions of the Falkner-Skan Equation for Flow Past a Stretching Boundary," *SIAM Journal on Applied Mathematics*, **49**(5), 1350–1358. <http://www.jstor.org/stable/2102025>.
- Sachdev, P.L., Kudenatti, R.B., and Bujurke, N.M., 2008, "Exact Analytic Solution of a Boundary Value Problem for the Falkner-Skan Equation," *Studies in Applied Mathematics*, **120**(1), 1–16. <https://doi.org/10.1111/j.1467-9590.2007.00386.x>.

Saeed, U., and Rehman, M., 2013, "Haar Wavelet–quasilinearization Technique for Fractional Nonlinear Differential Equations," *Applied Mathematics and Computation*, **220**, 630–648. <https://doi.org/10.1016/j.amc.2013.07.018>.

Sorrenti, M., Sciuva, M.D., Majak, J., and Auriemma, F., 2021, "Static Response and Buckling Loads of Multilayered Composite Beams Using the Refined Zigzag Theory and Higher-Order Haar Wavelet Method," *Mechanics of Composite Materials*, **57**(1), 1–18. <https://doi.org/10.1007/s11029-021-09929-2>.

Srinivasacharya, D., and Jagadeeshwar, P., 2017, "Flow Over an Exponentially Stretching Sheet with Hall, Thermal Radiation and Chemical Reaction Effects," *Frontiers in Heat and Mass Transfer*, **9**(37), 1–10. <http://dx.doi.org/10.5098/hmt.9.37>.

Takhar, H., Chamkha, A., and Nath, G., 2001, "Unsteady Three-dimensional MHD-Boundary-layer Flow due to the Impulsive Motion of a Stretching Surface," *Acta Mechanica*, **146**(1), 59–71. <https://doi.org/10.1007/BF01178795>.

Wang, C.Y., 1984, "The three-dimensional flow due to a stretching flat surface," *The Physics of Fluids*, **27**(8), 1915–1917. <https://aip.scitation.org/doi/abs/10.1063/1.864868>.

Weyl, H., 1942, "On the Differential Equations of the Simplest Boundary Layer Problem," *Annals of Mathematics*, **43**, 381–407. <https://doi.org/10.2307/1968875>.